American Mineralogist, Volume 86, pages 1267–1274, 2001

The $Mg(Fe)SiO_3$ orthoenstatite-clinoenstatite transitions at high pressures and temperatures determined by Raman-spectroscopy on quenched samples

PETER ULMER* AND ROLAND STALDER†

Department of Earth Sciences, ETH-Zentrum, CH-8092 Zurich, Switzerland

ABSTRACT

The phase boundaries limiting the stability fields of the three different $Mg(Fe)SiO_3$ phases [orthoenstatite (Oen), low-temperature clinoenstatite (LCen), and high-pressure clinoenstatite (HCen)] that occur at the pressure-temperature conditions prevailing in the Earth's upper mantle are inferred from Raman spectroscopy on quenched samples from high *P-T* experiments. There are subtle but significant differences between the spectra of Oen and the spectra of samples quenched within the stability field of HCen or LCen. The most prominent differences are additional peaks at 369 and 431 cm^{-1} in the spectrum of Cen and a systematic shift of the peak at 236 cm^{-1} in the Oen spectrum to 243 cm^{-1} in the Cen spectrum. However, no distinction can be made between samples quenched from the HCen and LCen stability fields. This is consistent with the fact that the HCen phase is non-quenchable and that the pyroxene phase observed in the experimental products is LCen as verified by powder X-ray diffraction.

Experiments performed in the pressure-temperature range 1.2–14 GPa and 750–1900 K have been used to constrain the $Mg(Fe)SiO_3$ phase diagram. Pyroxene compositions cover the range from pure $MgSiO_3$ to $Mg_{0.9}Fe_{0.1}SiO_3$ with minor amounts of Al, Ca, Na, and Cr. The results are similar to previous determinations from X-ray and optical studies and tightly constrain the HCen–Oen phase boundary, which can be expressed by the equation P (GPa) = 0.00454 T (K) + 1.673. The LCen–Oen boundary is not as well constrained, but the data are sufficient to locate the invariant point where all three $MgSiO_3$ phases coexist at 6.6 GPa and 820 °C.

INTRODUCTION

Enstatitic low-Ca pyroxene is the second most important phase in the Earth's upper mantle. Knowledge of stability fields and phase transitions that occur under conditions prevailing in the upper mantle are essential for the determination of the stable mineral assemblages that form under variable *P-T* conditions in the upper mantle. This in turn has profound impact on processes such as subduction, partial melting, or the occurrence of seismic discontinuities. The occurrence of several polymorphs of $MgSiO_3$ at mantle conditions has been demonstrated experimentally and confirmed from natural samples. Clinoenstatite in high-pressure ultramafic rocks has been described from Australia and the Alps (e.g., Trommsdorff and Wenk 1968; Bozhilov et al. 1999). The phase transition of clinoenstatite has been determined at low pressures (Grover 1972), up to 4 GPa (Boyd and England 1965) and from 2 to 12 GPa (Sclar et al. 1964) and consistently give relatively steep *P-T* slopes between 0.022 (Grover 1972) and 0.0385 GPa/K (Boyd and England 1965). From previous studies (Morimoto et al. 1960) it can be inferred that the lower pressure experiments (up to 4 GPa) produced a clinopyroxene with space group $P2_1/c$. The more recent experimental results of Yamamoto and Akimoto (1977) and Pacalo and Gasparik (1990) at pressures exceeding 5 GPa constrain the phase boundary between clinoenstatite and orthoenstatite to much higher temperatures at high pressures and give flat slopes of 0.0044 and 0.0031 GPa/K, respectively. Chopelas and Boehler (1992) and Angel et al. (1992) performed in situ single crystal Raman spectroscopy and X-ray experiments on $MgSiO_3$ pyroxenes in a diamond anvil cell up to 17 and 8 GPa respectively. They observed a first order non-quenchable phase transition from low–pressure orthoenstatite or $P2_1/c$ clinoenstatite (LCen) to a high-pressure clinoenstatite with space group $C2/c$ (HCen), the same as Ca-rich diopsidic clinopyroxenes. Similar phase relations with a low pressure $P2_1/c$ and a high pressure $C2/c$ clinopyroxene were documented for systems that contained Mn^{2+} and Cr^{2+} in addition to Mg (Arlt et al. 1998, 2000). Angel et al. (1992) and Angel and Hugh-Jones (1994) proposed a phase diagram for $MgSiO_3$ pyroxenes (summarized in Fig. 1) that is based on available experimental data on $MgSiO_3$ compositions cited above plus additional experimental constraints (Khodyrev and Agoshkov 1986; Wunder and Schreyer 1992, 1997; Luth 1995). For comparison, the orthoferrosilite (Ofs)/high-pressure clinoferrosilite (HCfs) boundary determined by Woodland and Angel (1997) is also shown on Figure 1.

The determination of the phase diagram is based on two different sets of experimental data: (1) Powder X-ray diffraction and optical studies performed on quenched samples from

* E-mail: peter.ulmer@erdw.ethz.ch
† Present address: Naturhistoriska riksmuseet, Sektionen för mineralogi, Box 50007, SE-10405 Stockholm, Sweden.

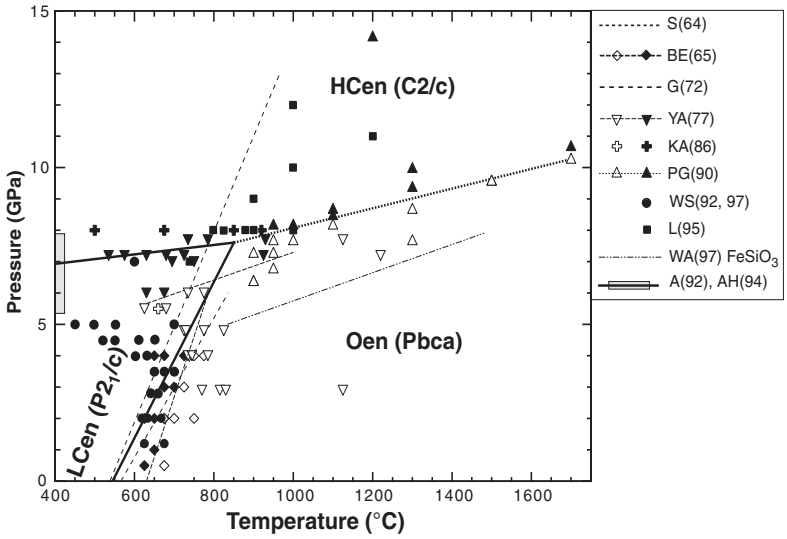

FIGURE 1. Summary of previous experimental data and phase relations of $MgSiO_3$ pyroxenes. Open symbols correspond to orthoenstatite; filled symbols are clinoenstatites. Data for $MgSiO_3$ are from: S(64) = Sclar et al. (1964); BE(65) = Boyd and England (1965); G(72) = Grover (1972); YA(77) = Yamamoto and Akimoto (1977); KA(86) = Khodyrev and Agoshkov (1986); PG(90) = Pacalo and Gasparik (1990); WS(92,97) = Wunder and Schreyer (1992, 1997); L(95) = Luth (1995). The orthoferrosilite to high-pressure clinoferrosilite transition of Woodland and Angel (1997) [WA(97)] is given for comparison. The shaded gray field on the y axes indicates room temperature (298 K) reversals for the HCen–LCen transition from Angel et al. (1992) and Angel and Hugh-Jones (1994) [A(92) and AH(94)]. The thick lines are the phase boundaries for the three enstatite polymorphs given by Angel and Hugh-Jones (1994).

high-pressure, high-temperature experiments in synthetic MgO-$SiO_2 \pm H_2O$ systems (Yamamoto and Akimoto 1977; Pacalo and Gasparik 1990) and with natural peridotite-like starting materials (Khodyrev and Agoshkov 1986). Woodland (1998) and Ross and Reynard (1999) provided additional data for intermediate (Mg,Fe)SiO_3 pyroxenes. (2) High-pressure in situ single crystal X-ray diffraction (Angel et al. 1992; Angel and Hugh-Jones 1994) and Raman spectroscopic studies (Chopelas and Boehler 1992; Chopelas 1999) to determine the LCen/HCen boundary. The two approaches require either relatively large amounts of $MgSiO_3$ pyroxene powder (powder X-ray diffraction) or (untwinned) single crystals of at least several tens of micrometers in size.

Here we report an alternative method to obtain information on the "structural state" of (Mg,Fe)SiO_3 pyroxenes from quenched high-pressure, high-temperature experimental samples. Inspection of Raman spectra of enstatitic pyroxenes from quenched samples revealed subtle but significant and consistent differences between experiments quenched within the Oen stability field and samples quenched within the LCen or HCen stability fields as depicted in Figure 1. The experiments cover a large *P-T* range from 1.2 to 14 GPa and 500–1600 °C. A variety of synthetic and natural starting compositions that either have "mantle-like" bulk compositions or represent primary magma compositions that are in equilibrium with a peridotitic residue have been used in this study. To put tighter constraints on the Oen/HCen and Oen/LCen boundaries, we performed some additional experiments in the synthetic MgO(FeO)-SiO_2-H_2O system and with natural serpentinized lherzolite material.

RAMAN SPECTROSCOPY OF QUENCHED (MG,FE)SiO_3 PYROXENES

The Raman spectra were acquired with a confocal Dilor LabRam II Micro-Raman spectrometer using a HeNe-laser with a wavelength of 632.8 nm in the range 100–1150 cm^{-1} and counting times of 500–1000s. Compared to X-ray diffraction experiments, micro-Raman spectroscopy has the advantage that extremely small amounts of material can be analyzed. A single grain of a few micrometers in size is enough to obtain a good spectrum. This allows us to analyze samples that contain just a few grains of minute enstatitic pyroxenes that we would not be able to separate and analyze by X-ray techniques or by optical microscopy. In addition, we can perform a full chemical analysis with the electron microprobe on the same small grain that we have analyzed by Raman-spectroscopy. Consequently, we were able to use samples that had bulk compositions far away from (Mg,Fe)SiO_3 and contained a few grains of pyroxene in addition to other phases. Table 1 and Figures 2 and 3 summarize the results of the systematic investigation of Raman spectra of enstatitic pyroxenes from a total of more than 60

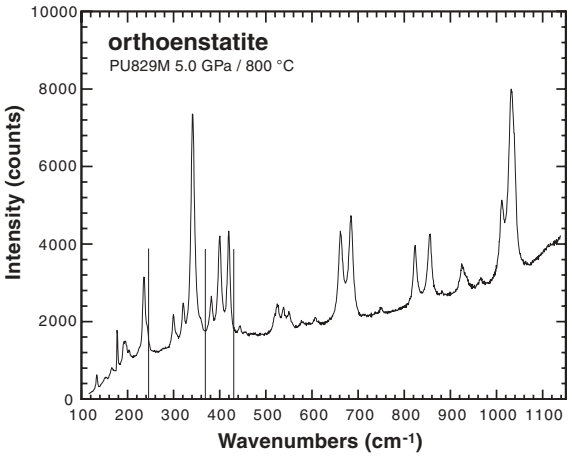

FIGURE 2. Representative Raman spectroscopic pattern of $MgSiO_3$ orthopyroxene (Oen). Thin vertical lines indicate the position of peaks that occur in the Cen pattern that are shifted (from 236 to 243 cm^{-1}) or absent (369 and 431 cm^{-1}) in the Oen pattern.

TABLE 1. Raman active vibrational modes of enstatitic pyroxenes

System	orthoenstatites				clinoenstatites				Hu00		Ch99	Ch99
Modes	MSH	Std. Dev.	Nat. Comp.	Std. Dev.	MSH	Std. Dev.	Nat. Comp.	Std. Dev.	$En_{.975}$	$En_{.90}$	Oen	Cen
#points	23		32		22		33					
υ_1	133.9	0.7	134.1	1.1	134.3	0.8	134.5	0.5			134	
υ_2	152.9	1.2	152.7	1.8	155.1	0.5	153.4	1.1			153	
υ_3	178.4	0.6	178.8	0.7	178.8	0.6	178.8	0.6				173
υ_4	195.9	1.3	191.9	1.3	194.6	0.9	192.4	0.8			193	
υ_5	204.6	1.4	200.1	0.7	203.4	1.8	200.2	0.9			206	217
υ_6	236.3	0.8	235.0	1.4	**233.5**	**1.0**	**232.4**	**1.0**	239	235	239	**229**
υ_{6c}					**243.7**	**1.4**	**242.3**	**1.1**				**253**
υ_7	276.2	1.8	274.4	2.2	277.4	1.3	275.3	2.1			279	
υ_8	300.3	1.0	298.5	1.1	301.3	1.2	298.4	1.4	304	297	302	
υ_9	322.5	1.3	319.9	1.2	323.2	1.1	321.2	1.2			323	320
υ_{10}	342.8	0.7	340.7	1.5	341.8	0.8	339.9	1.1	343	341	343	
υ_{11o}	**358.7**	**0.9**	**356.0**	**1.4**							**353**	
υ_{11c}					**369.0**	**0.6**	**367.0**	**1.4**				**366**
υ_{12}	382.4	0.7	379.8	1.5	385.3	1.7	383.5	1.7			384	378
υ_{13}	400.8	1.1	398.5	1.1	403.1	1.1	399.3	1.5	402	400	402	
υ_{14}	420.6	1.2	416.1	1.5	417.3	1.0	415.3	1.1	421		422	
υ_{14c}					**430.8**	**0.8**	**428.6**	**1.1**				
υ_{15}	444.4	1.4	441.7	2.3	451.5	1.3	449.7	1.8	446	441	446	452
υ_{16}	526.4	1.2	523.0	1.3	525.4	1.6	523.1	1.1	523	521	528	529
υ_{17}	539.5	0.9	538.3	1.6	542.1	1.1	540.7	1.5	541	537	540	
υ_{18}	551.9	1.3	549.5	1.9	554.0	0.9	553.0	1.1	552	549	553	
υ_{18c}					**581.4**	**1.4**	**578.5**	**1.8**	583			
υ_{19}	663.9	1.1	661.5	1.3	664.8	0.6	662.8	1.1	663	662	665	
υ_{20}	685.8	1.2	683.4	1.2	688.3	0.7	685.3	1.1	686	683	687	681
υ_{21}	749.2	1.4	749.3	1.7	753.5	1.4	751.6	2.5	750	746	751	751
υ_{22}	824.8	0.9	823.3	1.3	824.9	1.8	822.9	1.2				829
υ_{23}	856.2	1.4	855.0	2.4	846.9	1.6	853.2	1.9	854	857	853	
υ_{24}	929.1	2.6	929.2	2.0	927.4	2.2	929.0	3.0	933	938	937	914
υ_{25}	1012.6	1.2	1010.3	1.2	1012.5	0.7	1010.1	0.5	1013	1010	1014	1006
υ_{26}	1032.8	0.9	1030.2	2.0	1032.7	0.8	1029.1	1.5	1033	1025	1034	1024

Notes: Abbreviations: MSH = MgO-SiO_2-H_2O system; Nat. Comp. = "Peridotite-like" compositions (olivine-serpentinites Mg159 and CA1, group II kimberlite experiments, K-rich lherzolites, KNCMASH-system, and OlTi experiments); Std. Dev. = standard deviations; Oen = orthoenstatite; Cen = clinoenstatite; Hu00 = Huang et al. (2000); Ch99 = Chopelas (1999). For details of starting compositions see Table 2.

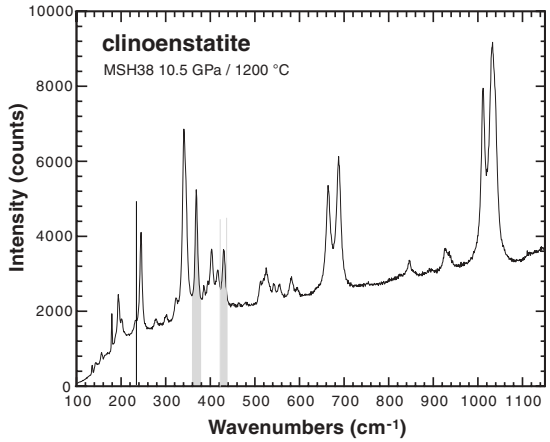

FIGURE 3. Representative Raman spectroscopic pattern of $MgSiO_3$ clinopyroxene (Cen). The vertical lines indicate the position of the peak in the Oen pattern that is shifted to 236 cm^{-1}. The shaded peaks are additional peaks that only occur in the Cen pattern (369 and 431 cm^{-1}).

high-pressure, high-temperature experiments. Figure 2 shows a typical orthoenstatite spectrum (x_{Mg} = 0.988) obtained at 5 GPa and 800 °C. This spectrum is virtually identical to those reported by Huang et al. (2000) for an x_{Mg} of 0.975 and Chopelas (1999) for pure enstatite. Figure 3 displays the Raman spectrum of an enstatite from an experiment at 10.5 GPa and 1200 °C, i.e., quenched within the stability field of HCen according to the data presented in Figure 1. There are small but significant differences between the two spectra. The Raman mode at 236 cm^{-1} in Oen is shifted to 244 cm^{-1}. More prominent additional peaks at 369 and 431 cm^{-1} are always present in experiments quenched within either the HCen or LCen stability fields and always absent in experiments quenched within the Oen stability field. Table 1 gives a summary of the Raman modes of enstatite observed in the experimental samples used to constrain the (Mg,Fe)SiO_3 phase diagram in this study. The Oen spectra obtained from this study are consistent with those of Huang et al. (2000) in that the slightly more Fe-rich pyroxenes from natural starting materials or synthetic systems that contain Fe show small but systematic shifts of the Raman modes. Most modes shift to lower wavenumbers consistent with the study by Huang et al. (2000) who observed negative dependence of the Raman modes with increasing Fe-content, except for the modes at 854 and 933 cm^{-1}. The pyroxenes used in this study cover a narrow range of compositions from x_{Mg} = 1.000 to 0.894. The spectra obtained from samples quenched within the Cen stability fields show the same small dependence on composition: the pure MSH samples give slightly higher wavenumbers than the "natural" samples for all observed modes, except ν23 and ν24. A comparison with the "real" HCen Raman modes reported by Chopelas and Boehler (1992), Chopelas (1999), and Ross and Reynard (1999) from in situ

high pressure studies in a diamond anvil cell shows that the Cen spectra observed in this study are intermediate between the Oen and "real" HCen spectra. The additional modes are present, but we still observe most, if not all, of the Oen modes. As expected, we do not observe significant differences between the Raman spectra recorded from samples quenched within the HCen or the LCen stability fields. Angel et al. (1992) and Angel and Hugh-Jones (1994) have demonstrated that the HCen phase is not quenchable, as it reverts to the LCen structure upon pressure release at room temperature. Therefore, the Cen Raman spectra recorded by us most probably corresponds to LCen or to a mixture of HCen and LCen spectra that cannot be differentiated. This is further supported by X-ray powder diffraction studies on Cen samples. We obtain identical low-clinoenstatite X-ray diffraction patterns for samples that have been quenched within the low-pressure or the high-pressure Cen stability fields. In summary, Raman spectroscopy of enstatitic clinopyroxene allows to differentiate between Oen and Cen but no further distinction between LCen ($P2_1/c$) and HCen ($C2/c$) can be made. As a consequence, we cannot directly determine the LCen/HCen boundary with this technique. However, the change in slope between the Oen/LCen and Oen/HCen boundaries can be used to put constraints on the location of the invariant point in the $MgSiO_3$ pyroxene system.

HIGH-PRESSURE HIGH-TEMPERATURE EXPERIMENTS USED IN THIS STUDY

We used a large number of experiments from a variety of studies of peridotite-like bulk compositions to constrain the enstatite phase diagram. The different studies were used to delimit: (1) the stability of hydrous phases and the fluid compositions in synthetic peridotite analogues in the MgO-(FeO)-SiO_2-H_2O system (Stalder and Ulmer 2001; Stalder et al. 2001) and in natural serpentinites (Ulmer and Trommsdorff 1995, 1999); and (2) the stability and phase relations of K-hydrosilicates in synthetic K_2O-Na_2O-CaO-MgO-Al_2O_3-SiO_2-H_2O and natural K-rich peridotites (Konzett and Ulmer 1999). Additional unpublished experiments on the phase relations of natural micaceous kimberlites (orangeites) and the solubility of TiO_2 in mantle olivine have also been used. Table 2 lists the bulk compositions of the starting materials used in the various experimental studies and Table 3 gives a summary of the experimental conditions and results. A limited number of additional experiments with synthetic MgO-(FeO)-SiO_2-H_2O[1] and natural serpentinite (CA1) starting materials were performed to provide tighter constraints on the Oen–Cen boundaries and to present nearly pure Mg-endmember enstatites with natural Fe-Al-Ca bearing enstatites under identical experimental conditions.

The experiments reported in Table 3 were conducted in the solid-media high-pressure laboratory of the Department of Earth Sciences at ETH Zurich. Starting material consisted of either natural serpentinites (CA1 and Mg159c, Table 2) or oxide, silicate, and carbonate mixtures that were ground under alcohol to less than 5–10 μm grain size. Water was either contained in the natural hydrous silicates (serpentine, brucite), or added as synthetic silicates and/or hydroxides (brucite, talc, phlogopite, and K-richterite amphibole). We used Au, $Au_{50}Pd_{50}$, and Pt capsules as well as graphite crucibles welded in Pt-capsules. Capsule sizes varied between 1.6 mm OD (1.4 mm ID) for the multi-anvil experiments and 2.3 mm OD (2.0 mm ID) for most piston cylinder and some multi-anvil experiments. Platinum capsules (3.00 and 4.00 mm diameter) were used for the graphite-Pt double capsule experiments. All capsules were welded shut and checked for leaks prior to the experiments. The presence of fluid was checked by weighing, piercing, drying, and

[1] Microprobe analyses of the synthetic talc used for the MgO-SiO_2-H_2O system revealed that the talc contains small amount of Fe and Ti. The x_{Mg} of the bulk MgO-SiO_2-H_2O mixture (tlc-bru) is 0.989 and the synthesized enstatites vary between 0.966 and 0.990 depending on modal amount and coexisting phases.

TABLE 2. Compositions of starting materials used in experiments to constrain the Oen–Cen boundaries

Sample	CA1	Mg159c	KNCMASH	KL5phl	KL10kr	GPII	OlTi	tlc-bru	fo-tlc
Material	natural	natural	synthetic	synthetic	synthetic	synthetic	synthetic	synthetic	synthetic
Reference	S99	UT95	KU99	KU99	KU99	u.p.	u.p.	SU01	u.p.
SiO_2	40.99	43.32	47.28	45.35	46.56	35.48	38.45	43.36	57.78
TiO_2	0.04	0.00	0.00	0.12	0.12	1.00	3.00	0.00	0.00
Al_2O_3	2.16	1.30	11.50	4.37	3.60	3.16	0.00	0.00	0.00
Fe_2O_3	7.67	0.50	0.00	0.00	0.00	0.00	0.00	0.00	0.00
FeO	n.d.	2.59	0.00	6.95	6.66	8.22	10.28	0.00	0.00
MnO	0.08	0.04	0.00	0.08	0.07	0.24	0.00	0.00	0.00
MgO	36.08	39.62	27.26	37.24	36.47	29.10	47.33	43.63	38.76
CaO	2.37	0.00	6.58	3.55	4.00	5.88	0.00	0.00	0.00
Na_2O	0.01	0.00	1.22	0.69	1.08	0.93	0.00	0.00	0.00
K_2O	0.01	0.00	4.94	0.54	0.38	3.17	0.00	0.00	0.00
P_2O_5	0.01	0.00	0.00	0.00	0.00	0.00	0.00	0.00	0.00
Cr	0.34	0.23	0.00	0.69	0.66	0.30	0.00	0.00	0.00
Ni	0.31	0.08	0.00	0.21	0.20	0.44	0.00	0.00	0.00
L.O.I.	10.17	n.d.	n.d.	n.d.	n.d.	n.d.	n.d.	n.d.	n.d.
H_2O	n.d.	*12.10	1.22	0.21	0.20	4.97	0.94	13.00	3.46
CO_2	n.d.	n.d.	0.00	0.00	0.00	7.13	0.00	0.00	0.00
Total	100.24	99.78	100.00	100.00	100.00	100.02	100.00	100.00	100.00
xMg	0.903	0.959	1.000	0.905	0.907	0.863	0.891	1.000	1.000

Notes: References: S99 = Schönbächler (1999); UT95 = Ulmer and Trommsdorff (1995); KU99 = Konzett and Ulmer (1999); SU01 = Stalder and Ulmer (2001); Stalder et al. (2001); u.p. = Unpublished data of our laboratory. Abbreviations: n.d. = not determined; *x* Mg = molar MgO/(FeO_{tot} + MgO).
* H_2O content calculated assuming stoichiometry and charge balance basing on the antigorite formula $Mg_{48}Si_{34}O_{85}(OH)_{62}$ (Mellini et al. 1987).

TABLE 3. Run conditions and results of high pressure experiments

Run no.	*T* (°C)	*P* (GPa)	start. mat.	Time (h)	App.	product phases
MgO – SiO_2 – H_2O (MSH) System						
PU712	900	1.2	fo-tlc	41.0	PC	Oen
PU827M	750	5.0	tlc-bru	54.2	MA	Cen fo chum fluid
PU829M	800	5.0	tlc-bru	48.0	MA	Oen fo chum fluid
MSH49	900	5.0	tlc-bru	48.0	MA	Oen fo chu fluid
MSH51	975	5.0	tlc-bru	24.0	MA	Oen fo chu fluid
MSH48	1050	5.0	tlc-bru	18.0	MA	Oen fo fluid
MSH55	800	6.0	tlc-bru	72.0	MA	O/Cen? fo chu fluid
PU823M	800	7.2	tlc-bru	26.7	MA	Cen fo chum fluid
PU824M	875	7.2	tlc-bru	24.9	MA	Cen fo chum fluid
PU826M	925	7.2	tlc-bru	28.2	MA	Cen fo chum fluid
PU828M	975	7.2	tlc-bru	24.0	MA	Oen fo chum fluid
PU830M	1100	8.2	tlc-bru	27.8	MA	Cen fo liq
PU831M	1150	8.2	tlc-bru	10.6	MA	Cen fo liq
PU832	1200	8.2	tlc-bru	1.0	MA	Oen fo liq
MSH17	1150	9.0	tlc-bru	6.0	MA	Cen fo liq
MSH38	1200	10.5	tlc-bru	3.0	MA	Cen fo liq
Serpentinites Mg159c & CA1						
PU711	710	1.8	159	207.7	PC	Oen fo chl (tlc)
PU544	730	2.5	159	70.6	PC	Oen fo chl (atg)
PU545	710	3.0	159	71.0	PC	Oen fo chl (atg)
PU741	800	3.0	CA1	99.5	PC	Oen fo gar
PU725	820	3.0	CA1	136.3	PC	Oen fo gar
PU721	860	3.0	CA1	120.6	PC	Oen fo gar
PU550	670	4.0	159	40.8	MA	Cen fo chl (atg)
PU507	660	4.5	159	5.5	MA	Cen fo chl fluid
PU827C	750	5.0	CA1	54.2	MA	Cen fo gar fluid
PU829C	800	5.0	CA1	48.0	MA	Oen fo gar fluid
PU555	630	5.4	159	30.0	MA	Cen fo (chl atg)
PU809	800	6.1	CA1	74.3	MA	Cen fo gar fluid
PU820	800	6.1	CA1	115.0	MA	Cen/Oen fo fluid
PU565	600	6.2	159	11.0	MA	Cen fo (atg)
PU571	560	7.1	159	30.0	MA	Cen A 10Å
PU823C	800	7.2	CA1	26.7	MA	Cen fo gar fluid
PU824C	875	7.2	CA1	24.9	MA	Cen fo gar fluid
PU826C	925	7.2	CA1	28.2	MA	Cen fo gar fluid
PU828C	975	7.2	CA1	24.0	MA	Oen fo gar fluid
PU519	500	7.7	159	8.0	MA	Cen A fluid
PU784	700	8.0	CA1	34.1	MA	Cen A fluid
PU830C	1100	8.2	CA1	27.8	MA	Cen fo gar fluid/liq
PU831C	1150	8.2	CA1	10.6	MA	Cen fo gar fluid/liq
PU791	900	12.0	CA1	26.7	MA	Cen chum E gar fluid
PU788	1100	12.0	CA1	24.0	MA	Cen fo gar liq
GPII kimberlite, K-lherzolite & KNCMASH Systems						
PU619	1100	7.0	KL5phl	4.3	MA	Oen cpx fo gar fluid
MA24	1150	7.5	GPII	0.7	MA	Oen fo gar cpx mag liq
MA25	1200	7.5	GPII	0.5	MA	Oen fo gar cpx liq
MA22	1250	7.5	GPII	0.3	MA	Oen fo gar liq
MA23	1300	7.5	GPII	0.5	MA	Oen fo gar liq
MA106	1300	8.0	KNCMASH	24.7	MA	Oen cpx fo gar liq
PU649	1200	8.0	KL5phl	51.6	MA	Oen cpx fo gar Kr
PU642	1200	8.0	GPII	23.0	MA	Oen cpx fo gar mag
PU645	1300	8.0	KL5phl	42.6	MA	Oen cpx fo gar liq
PU659	1300	8.0	KL10kr	29.7	MA	Oen cpx fo gar liq
PU646	1500	8.0	GPII	1.0	MA	Oen fo gar liq
PU667	1200	9.5	KL10kr	27.3	MA	Cen cpx fo gar liq
PU652	1200	9.5	GPII	2.0	MA	Cen cpx fo gar mag liq
PU698	1300	9.5	KL10kr	7.7	MA	Cen cpx fo gar liq
PU653	1400	9.5	GPII	1.0	MA	Cen fo gar liq
PU655	1600	9.5	GPII	0.5	MA	Oen fo gar liq
OlTi (Fo90 – Ilm40 – En92) Experiments						
PU680	1400	2.0	OlTi1	8.0	PC	Oen fo rut liq
PU665	1400	4.0	OlTi1	26.8	MA	Oen fo rut liq
PU660	1400	6.0	OlTi1	23.7	MA	Oen fo rut liq
PU678	1400	7.5	OlTi1	2.7	MA	Oen fo rut liq
PU662	1400	9.0	OlTi1	23.0	MA	Oen fo ilm liq
PU733	1400	12.0	OlTi1	23.0	MA	Cen fo ilm liq
PU755	1400	14.0	OlTi1	23.5	MA	Cen fo wads liq

Notes: Starting materials (start. mat.) refer to Table 2. App: PC = piston-cylinder, MA = multi-anvil apparatus. Abbreviations for phases: Oen = orthoenstatite, Cen = clinoenstatite, fo = forsterite (olivine), cpx = clinopyroxene (high-Ca pyroxene), gar = garnet, liq = liquid phase (either glass or quench-crystals), mag = magnesite, chum = clinohumite, Kr = K-richterite amphibole, rut = rutile, ilm = ilmenite, wads = wadsleyite, A = phase A, E = phase E, 10Å = 10 Å phase. Product phases in parenthesis indicate phases only present in minor amounts.

weighing after the experiments except for fluid-undersaturated melting experiments in the K-hydrosilicate, micaceous kimberlite, and Ti-in-olivine experiments.

Piston cylinder experiments

At pressures of less than 3.5 GPa an end-loaded piston cylinder apparatus with a piston diameter of 14 mm was used. Assemblies consisted of NaCl or NaCl-Pyrex-MgO. Pt-$Pt_{90}Rh_{10}$ (type S) thermocouples were used. Assemblies were calibrated on the following reactions/phase transitions: fayalite + qtz = orthoferrosilite at 1.41 GPa and 1000 °C (Bohlen et al. 1980) and qtz = coesite at 3.2 GPa and 1200 °C (Bose and Ganguly 1995). Experiments were terminated by near isobaric quench with quench rates in the order of 200–400 °C/s.

Multi-anvil experiments

Experiments at pressures in excess of 3.5 GPa were performed in a 6/8 multi-anvil apparatus using tungsten carbide cubes with truncation edge lengths (TEL) of 8, 11, 12, and 17 mm depending on pressure range and sample volume. Stepped graphite heaters were used to 9 GPa and stepped $LaCrO_3$-heaters at higher pressures. Assemblies were calibrated at room temperature against the phase transition in Bi and Ba metal. High temperature calibrations were based on the following phase transitions: SiO_2 = qtz – coesite (3.2 GPa, 1200 °C, Bose and Ganguly 1995); Fe_2SiO_4 = fayalite – γ-spinel (5.25 GPa, 1000 °C, Yagi et al. 1987); $CaGeO_3$ = garnet – perovskite (6.1 GPa, 1200 °C, Susaki et al. 1985); TiO_2 = rutile – α-PbO_2-structure (7.7 GPa, 1100 °C, Akaogi et al. 1992); SiO_2 = coesite – stishovite (9.3 GPa, 1200 °C, Yagi and Akimoto 1976; Zhang et al. 1996); Mg_2SiO_4 = α – β-transition (14.5 GPa, 1400 °C, Morishima et al. 1994). Temperatures were measured with Pt/$Pt_{90}Rh_{10}$ and WRe_5-WRe_{26} thermocouples; reported temperatures are uncorrected for the effect of pressure on the thermocouple EMF. Experiments were terminated by isobaric quench with quenching rates in the order of 500–700 °C/s.

Most recovered samples were embedded in epoxy mounts and polished to expose longitudinal cross sections; samples were examined under a reflecting light microscope and phases were identified by Raman spectroscopy and with an electron microprobe (Cameca SX50). From a few (older) samples only powders that were used for X-ray diffraction studies were available. Small aliquots of the powders were dispersed with alcohol on glass holders and directly measured on the Raman spectrometer.

PU823C/M through PU831C/M and PU832 were additional experiments performed for this study. Two capsules of 1.6 mm OD and 1.4–1.8 mm in length were loaded simultaneously for experiments PU823-831 (Table 3). The letter C denotes experiments with the natural serpentinite starting material CA1, and M corresponds to experiments with the talc-brucite synthetic starting material. These experiments were designed to delimit the Oen–Cen boundary at 5, 7.2, and 8.2 GPa and to evaluate the influence of pure $MgSiO_3$ vs. "natural" Fe-bearing mantle pyroxenes.

RESULTS

The results of the experimental studies bearing on the Oen–H/LCen boundaries are presented in Tables 3 and 4 and in Fig-

TABLE 4. Representative low-Ca pyroxene analysis of MSH, CA1, GPII, and Ti-olivine experiments

System			MSH				CA1			GPII			OlTi
Sample	PU826	PU829	PU832	PU831M	PU741	PU788	PU831C	PU828C	PU653	PU655	MA24	PU677	PU733
	Cen	Oen	Oen	Cen	Oen	Cen	Cen	Oen	Cen	Oen	Oen	Oen	Cen
SiO_2	59.67	59.59	59.37	60.18	55.33	57.83	58.02	58.48	57.20	58.06	55.96	58.32	58.50
TiO_2	n.d.	n.d.	0.00	0.00	0.06	0.00	0.05	0.01	0.07	0.07	0.15	0.28	0.22
Cr_2O_3	n.d.	n.d.	0.00	0.00	0.20	0.11	0.00	n.d.	0.08	0.14	0.17	n.d.	n.d.
Al_2O_3	n.d.	n.d.	0.18	0.19	3.08	0.20	1.40	0.27	0.23	0.63	0.44	n.d.	0.24
Fe_2O_3	0.00	0.00	0.39	0.15	0.83	1.68	0.48	0.00	3.07	0.22	4.24	0.00	0.00
FeO	2.37	0.85	0.12	0.64	5.48	2.29	2.28	4.85	2.39	4.69	3.58	5.44	4.73
MnO	n.d.	n.d.	0.00	0.01	0.15	0.05	0.03	0.13	0.09	0.11	0.13	n.d.	0.01
MgO	37.73	38.82	39.73	39.96	33.89	37.48	37.49	36.22	36.15	34.53	34.90	36.13	36.41
CaO	n.d.	n.d.	0.01	0.01	0.14	0.01	0.09	0.05	0.59	1.67	0.55	n.d.	0.01
Na_2O	n.d.	n.d.	0.01	0.01	0.00	0.00	0.02	0.01	0.10	0.19	0.06	n.d.	0.00
Total	99.77	99.26	99.81	101.15	99.16	99.65	99.86	100.02	99.97	100.31	100.18	100.17	100.12
Cations basing on four cations and six O atoms													
Si	2.024	2.017	1.992	1.995	1.922	1.973	1.967	1.998	1.961	1.989	1.933	1.995	1.996
Ti	n.d.	n.d.	0.000	0.000	0.002	0.000	0.001	0.000	0.002	0.002	0.004	0.008	0.006
Cr	n.d.	n.d.	0.000	0.000	0.006	0.003	0.000	0.000	0.002	0.004	0.005	n.d.	n.d.
Al	n.d.	n.d.	0.007	0.007	0.126	0.008	0.056	0.011	0.009	0.025	0.018	n.d.	0.010
Fe^{3+}	0.000	0.00	0.010	0.004	0.022	0.043	0.012	0.000	0.079	0.006	0.110	0.000	0.000
Fe^{2+}	0.067	0.024	0.004	0.018	0.159	0.065	0.065	0.139	0.069	0.134	0.104	0.156	0.135
Mn	n.d.	n.d.	0.000	0.000	0.004	0.001	0.001	0.004	0.003	0.003	0.004	n.d.	0.001
Mg	1.908	1.959	1.987	1.975	1.755	1.906	1.893	1.845	1.846	1.762	1.797	1.842	1.852
Ca	n.d.	n.d.	0.001	0.001	0.005	0.001	0.003	0.002	0.022	0.061	0.020	n.d.	0.001
Na	n.d.	n.d.	0.000	0.001	0.000	0.000	0.001	0.001	0.006	0.013	0.004	n.d.	0.000
x_{Mg}	0.966	0.988	0.984	0.989	0.907	0.946	0.961	0.930	0.926	0.926	0.894	0.922	0.932

Notes: n.d. = not determined; $x_{Mg} = Mg/(Mg + Fe_{tot})$; MSH, CA1, GPII, and OlTi refer to Table 2.

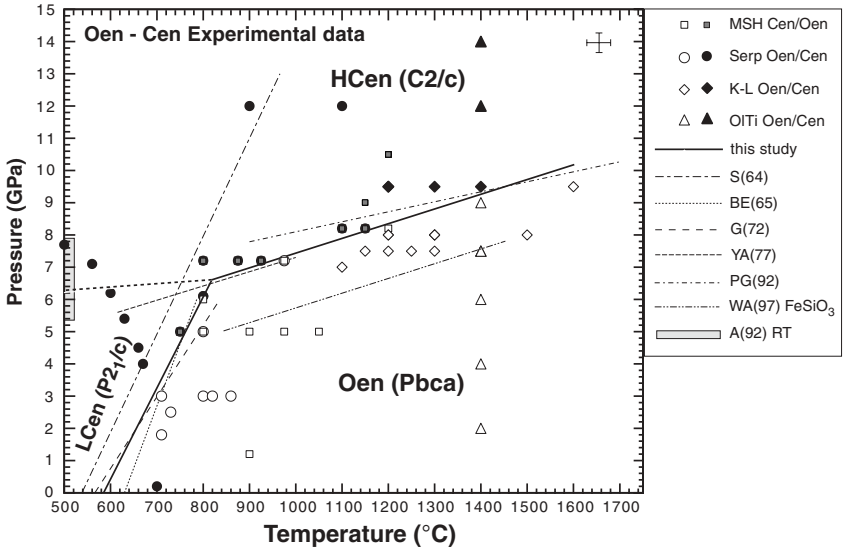

FIGURE 4. Pressure-temperature phase diagram for $(Mg,Fe)SiO_3$ pyroxenes showing the positions of the present experiments. Open symbols correspond to orthoenstatite; filled symbols are clinoenstatites. Abbreviations correspond to starting materials used (Table 2): MSH = fo-tlc and tlc-bru; Serp = CA1 and Mg159c; K-L = KNCMASH, KL5phl, KL10kr, and GPII, OlTi = OlTi. Thick solid lines represent the Oen-HCen and Oen-LCen boundary constrained by the present experiments; the thick broken line indicates the LCen-HCen that has not been inferred by the present study. Thin lines represent previous studies on Oen-Cen stabilities, data sources and abbreviations are the same as in Figure 1. The cross in the upper right corner of the diagram indicates the estimated errors in pressure and temperature of the multi-anvil experiments.

ure 4. The compositions of enstatitic pyroxenes cover a narrow range from pure enstatite ($MgSiO_3$, $x_{Mg} = 1.00$) to low-Ca pyroxenes with up to 10% ferrosilite component ($x_{Mg} \leq 0.894$) and Al_2O_3 up to 1.4 wt%, CaO to 1.67 wt% (at 1600 °C). All other oxides are less than 0.3 wt%. Figure 4 shows the phase diagram resulting from Raman-spectroscopic investigation of the enstatitic pyroxenes. The Oen–HCen boundary is well constrained and has a rather flat slope. The LCen–Oen boundary is not as well constrained, but the data clearly indicate a much steeper slope than the HCen–Oen boundary. A comparison with previous determinations based exclusively on X-ray techniques or optical microscopy show that the general agreement is good. The HCen–Oen boundary determined in this study has a steeper slope than that previously determined by Pacalo and Gasparik (1990) (0.0031), but is identical to that determined by Yamamoto and Akimoto (1977) (0.0044). The HCen–Oen boundary is represented by the equation:

$$P\,(\text{GPa}) = 0.00454\,T(\text{K}) + 1.673 \quad (1)$$

There is no obvious explanation for the difference in slope of the Oen–HCen phase transition and consequently the transition-pressure at low temperatures between Pacalo and Gasparik (1990), Yamamoto and Akimoto (1977) and this study. Pacalo

and Gasparik (1990) performed reversal experiments using seed crystals of Cen and Oen and Pb-based fluxes. They determined the phase boundary by optical microscopy (changes of extinction and birefringence) of the seed and/or newly grown crystals. This study and the study by Yamamoto and Akimoto (1977) are synthesis experiments with no enstatite present in the starting material. Crystallization was promoted by hydrous fluid and/or hydrous silicate melt. Potential causes of the observed discrepancies in the location of the Oen/HCen phase boundary at lower temperatures are slow reaction kinetics and differences in design and pressure calibration of the multi-anvil presses used. Additional differences could arise from the use of hydrous fluids or melts in the present study, since different solubilities of OH in Oen and HCen might theoretically influence the location of the phase boundary. However, available data on the solubility of hydroxyl ions in both Oen (Kohn 1996) and HCen (Bolfan-Casanova et al. 2000) indicate very low solubilities in the order of 250 (Oen) to 600 ppm (HCen) that should not have detectable effects on the phase boundary.

The HCen–LCen boundary cannot be delimited by quench experiments, because the HCen structure inverts upon pressure release to the LCen structure. The LCen–Oen boundary was not investigated in great detail in this study. The available brackets, particularly at pressures of less than 4 GPa do not provide tight constraints, but the results are consistent with previous determinations (Boyd and England 1965; Grover 1972). To locate the invariant point (triple point) we performed additional experiments at 5.0, 6.1 and 7.2 GPa (Table 3) with both synthetic MSH and natural serpentinite starting materials. A best fit through the available data constrains the invariant point at approximately 6.6 GPa and 820 °C. Previous estimates were 7.6 GPa and 850 °C (Angel and Hugh-Jones 1994; Woodland 1998) about 1 GPa higher due to the flatter slope of the Oen–HCen transition proposed by Pacalo and Gasparik (1990).

A comparison with the $FeSiO_3$ orthoferrosilite–high-P clinoferrosilite transition determined by Woodland and Angel (1997) in reversal experiments reveals an identical slope (0.00454 vs. 0.00457) but a shift to lower pressures of 1.76 GPa. This implies that the exchange of Mg for Fe^{2+} affects only the pressure of the phase transition, but not the slope. The small variation of x_{Mg} in the present study would correspond to a maximum shift of the Oen–HCen boundary of 0.18 GPa. This is considered to be within the experimental uncertainty of 0.2 GPa. We could not detect any difference between experiments using nearly pure MgO-SiO_2-H_2O and natural serpentinites with a bulk x_{Mg} of 0.9 and the kimberlite with 0.863 (however all enstatitic pyroxenes in the kimberlite experiments exhibit x_{Mg} of ≥ 0.89). The most obvious examples are experiments PU826 and PU828 (Table 3) which bracket the Oen-HCen boundary at 7.2 GPa and approximately 950 °C. These experiments were performed with two capsules located above and below a central thermocouple inserted axially from the gasket fins. The two capsules should have been exposed to identical temperature and pressure conditions. They show the same pyroxene Raman spectra: Cen at 7.2 GPa/925 °C and Oen 7.2 GPa/975 °C. The x_{Mg} of the enstatitic pyroxene is 0.99 in the MSH experiments (M) and 0.93 in the CA1 (C) experiments. These experiments confirm that the addition of small amounts of Fe^{2+} to the Mg-rich system does not result in a significant shift of the Oen–HCen boundary. These results are consistent with those of Woodland (1998). He found a very narrow loop of coexisting cpx and opx for x_{Mg} 0.3–0.6. A reduction of the transition pressure at 1200 °C from 8.7 to 8.3 GPa resulting from the present study is consistent with the dataset of Woodland (1998). In conclusion, the location of the phase transition from orthorhombic to *C*2/*c* in low-Ca mantle pyroxenes that contain up to 10% ferrosilite component plus small amount of Al, Ca, Cr, Ti, and Na does not significantly differ from that of endmember $MgSiO_3$ pyroxene.

THERMODYNAMIC CONSIDERATIONS

A rigorous thermodynamic treatment of the Oen-HCen phase transition has not previously been possible because of inadequate thermodynamic and volumetric data for the non-quenchable HCen phase. Angel and Hugh-Jones (1994) and Hugh-Jones and Angel (1994) have determined the room-temperature compression of enstatitic pyroxenes and constrained an equation of state (EOS) for HCen at 298 K. There are no measurements of the thermal expansion or calorimetric determinations of the heat capacity (C_P) or enthalpy for the HCen phase. Chopelas (1999) provided an estimate of the entropy of reaction of the Oen/HCen transition of –2.8 J/(mol·K) based on the density of vibrational modes and the thermal expansion coefficient of forsterite. The resulting ΔV of reaction was –0.6 cm^3 mol^{-1} with a Clapeyron slope of 0.0031 GPa/K (Pacalo and Gasparik 1990). Angel and Hugh-Jones (1994) have calculated the entropy of reaction [ΔS_0, –2.59 J/(mol·K)] and the enthalpy of reaction (ΔH_0, 3.7 KJ/mol) at 298 K based on their EOS for Oen and HCen linearly extrapolated to 298 K and the Clapeyron slope determined by Pacalo and Gasparik (1990) (Table 5). Combining the $\Delta V_{P,298}$ of reaction of 0.836 cm^3/mol in the pressure range of 4 to 8 GPa as determined by Angel and Hugh-Jones (1994) and the slope of 0.00454 GPa/K [this study, equation (1)] we obtain a ΔS_0 of 3.80 J/(mol·K), about 50% larger than that of Angel and Hugh-Jones (1994). The enthalpy of reaction is obtained from the equation $\Delta G_0 = \Delta H_0 - T\Delta S_0 + P_{298}\Delta V_{P,298}$ by setting ΔG_0 to zero at the reaction boundary; P_{298} is the pressure of the reaction boundary linearly extrapolated to 298 K. Table 5 shows a comparison of the different values for $MgSiO_3$ and $FeSiO_3$ from this and previous studies. The

TABLE 5. Thermodynamic parameters of phase transitions in $(Mg,Fe)SiO_3$ pyroxenes

Source	$FeSiO_3$ Ofs → HCfs (Woodland and Angel 1997)	$MgSiO_3$ Oen → HCen (Angel and Hugh-Jones 1994)	$MgSiO_3$ Oen → HCen this study
$\delta P/\delta T$ (GPa/K)	0.00457	0.0031*	0.00454
ΔV_0 (cm^3)	–0.92	–0.900	–0.900†
$\Delta V_{P,298}$ (cm^3)	–0.90‡	–0.836§	–0.836§
P_{298} (GPa)	1.28	5.08*	3.03
ΔS_0 [J/(mol·K)]	–4.11	–2.59	–3.80
ΔH_0 (KJ/mol)	–0.076	+3.8‖	+1.40

* From Pacalo and Gasparik (1990).
† Values taken from Angel and Hugh-Jones (1994).
‡ At 0 to 5 GPa.
§ At 4 to 8 GPa.
‖ Corrected value reported by Woodland and Angel (1997).

slope and the ΔS_0 obtained in this study for the Oen to HCen transition are very similar to those obtained for pure $FeSiO_3$ (Woodland and Angel 1997). The enthalpy of reaction becomes considerably smaller than previously calculated with the steeper slope used by Angel and Hugh-Jones (1994). This implies that not only the mechanism of the ortho- to high-P clinopyroxene phase transition is identical in $MgSiO_3$ and $FeSiO_3$ but also the entropy and enthalpy changes associated with the phase transition are comparable within error.

ACKNOWLEDGMENTS

This project was supported by the Schweizer Nationalfonds, grant 2000-050661.97. We gratefully acknowledge Eric Reusser for assistance with microprobe analyses. Jürgen Konzett is thanked for providing some of the high-pressure samples used in this study. We thank Ann Chopelas and Bruno Reynard for their constructive reviews and comments.

REFERENCES CITED

Akaogi, M., Susaki, J.-I., Yagi, T., Matsui, M., Kikegawa, T., Yusa, H., and Ito, E. (1992) High-pressure-temperature stability of α-PbO_2-type TiO_2 and $MgSiO_3$ majorite; calorimetric and in situ diffraction studies. In Y. Syono and M.H. Manghnani, Eds. High Pressure Research: Application to Earth and Planetary Sciences, Geophysical Monograph, 67, p. 447–455. American Geophysical Union, Washington, D.C.

Angel, R.J. and Hugh-Jones, D.A. (1994) Equations of state and thermodynamic properties of enstatite pyroxenes. Journal of Geophysical Research, 99(B10), 19777–19783.

Angel, R.J., Chopelas, A., and Ross, N.L. (1992) Stability of high-density clinoenstatite at upper-mantle pressures. Nature, 358, 322–358.

Arlt, T., Angel, R.J., Miletich, R., Armbruster, T., and Peters, T. (1998) High-pressure $P2_1/c$-$C2/c$ phase transitions in clinopyroxenes: Influence of cation size and electronic structure. American Mineralogist, 83, 1176–1181.

Arlt, T., Kunz, M., Stolz, J., Armbruster, T., and Angel, R.J. (2000) P-T-X data on $P2_1/c$-clinopyroxenes and their displacive phase transitions. Contributions to Mineralogy and Petrology, 138, 35–45.

Bohlen, S.R., Essene, E.J., and Boettcher, A.L. (1980) Reinvestigation and application of olivine-qtz-opx barometry. Earth and Planetary Science Letters, 47, 1–10.

Bolfan-Casanova, N., Keppler, H., and Rubie, D.C. (2000) Water partitioning between nominally anhydrous minerals in the MgO-SiO_2-H_2O system to 24 GPa: Implications for the distribution of water in the Earth's mantle. Earth and Planetary Science Letters, 182, 209–221.

Bose, K. and Ganguly, J. (1995) Quartz-coesite transition revisited: Reversed experimental determinations at 500–1200 °C and retrieved thermochemical properties. American Mineralogist, 80, 231–238.

Boyd, F.R. and England, J.L. (1965) The rhombic enstatite-clinoenstatite inversion. Carnegie Institution Yearbook, 64, 117–120.

Bozhilov, K.N., Green, H.W., and Dobrzhinetskaya, L. (1999) Clinoenstatite in Alpe Arami peridotite: Additional evidence of very high pressure. Science, 284, 128–132.

Chopelas, A. (1999) Estimates of mantle relevant Clapeyron slopes in the $MgSiO_3$ system from high-pressure spectroscopic data. American Mineralogist, 84, 233–244.

Chopelas, A. and Boehler, R. (1992) Raman spectroscopy of high pressure MgSiO3 phases synthesized in a CO_2 laser heated diamond anvil cell: Perovskite and clinopyroxene. In Y. Syono, and M.H. Manghnani, Eds, High-Pressure Research: Application to Earth and Planetary Sciences, Geophysical Monograph, 67, p. 101–108. American Geophysical Union, Washington, D.C.

Grover, J. (1972) The stability of low-clinoenstatite in the system $Mg_2Si_2O_6$-$CaMgSi_2O_6$. EOS, Transactions of the American Geophysical Union, 53, 539.

Huang, E., Chen, C.H., Huang, T., Lin, E.H., and Xu, J.-A. (2000) Raman spectroscopic characteristics of Mg-Fe-Ca pyroxenes. American Mineralogist, 85, 473–479.

Hugh-Jones, D.A. and Angel, R.J. (1994) A compressional study of $MgSiO_3$ orthoenstatite up to 8.5 GPa. American Mineralogist, 79, 405–410.

Khodyrev, O.Y. and Agoshkov, V.M. (1986) Phase transitions in serpentine in the MgO-SiO_2-H_2O system at 40–80 kbar. Geochemistry International, 23 (7), 47–52.

Kohn, S.C. (1996) Solubility of H2O in nominally anhydrous mantle minerals using 1H MAS NMR. American Mineralogist, 81, 1523–1526.

Konzett, J. and Ulmer, P. (1999) The stability of hydrous potassic phases stability in lherzolitic mantle—an experimental study to 9.5 GPa in simplified and natural bulk compositions. Journal of Petrology, 40, 629–652.

Luth, R.W. (1995) Is phase A relevant to the Earth's mantle? Geochimica Cosmochimica Acta, 59, 679–682.

Mellini, M., Trommsdorff, V., and Compagnoni, R. (1987) Antigorite polysomatism: behavior during progressive metamorphism. Contributions to Mineralogy and Petrology, 97, 147–155.

Morimoto, N., Appleman, D.E., and Evans, J.H.T. (1960) The crystal structures of clinoenstatite and pigeonite. Zeitschrift für Kristallographie, 114, 120–147.

Morishima, H., Kato, T., Suto, M., Ohtani, E., Urakawa, S., Utsumi, W., Shimomura, O., and Kikegawa, T. (1994) The phase boundary between α- and β-Mg_2SiO_4 determined by in situ X-ray observation. Science, 265, 1202–1203.

Pacalo, R.E.G. and Gasparik, T. (1990) Reversals of the orthoenstatite—clinoenstatite transition at high pressures and temperatures. Journal of Geophysical Research, 95, 15853–15858.

Ross, N.L. and Reynard, B. (1999) The effects of iron on the $P2_1/c$ to $C2/c$ transitions in $(Mg,Fe)SiO_3$ clinopyroxenes. European Journal of Mineralogy, 11, 585–589.

Schönbächler, M. (1999) Die Hochdruckmetramorphose der Ultramafika und der angrenzenden Nebengesteine am Cerro de Almiréz, Sierra Nevada, Südspanien. Diploma thesis, Department of Earth Sciences, p. 113. ETH, Zurich.

Sclar, C.B., Carrison, L.C., and Schwartz, C.M. (1964) High pressure stability fields of clinoenstatite, and the orthoenstatite- clinoenstatite transition. EOS, Transactions of the American Geophysical Union, 45, 121.

Stalder, R. and Ulmer, P. (2001) Phase relations of a serpentine composition between 5 and 14 GPa—Significance of clinohumite and phase E as water carriers into the transition zone. Contributions to Mineralogy and Petrology, 140, 670–679.

Stalder, R., Ulmer, P., Thompson, A.B., and Günther, D. (2001) High pressure fluids in the system MgO-SiO_2-H_2O at upper mantle conditions. Contributions to Mineralogy and Petrology, 140, 607–618.

Susaki, J., Akaogi, M., Akimoto, S., and Shiomura, O. (1985) Garnet-Perovskite transformation in $CaGeO_3$: In-situ X-ray measurements using synchrotron radiation. Geophysical Research Letters, 12(10), 729–732.

Trommsdorff, V. and Wenk, H.-R. (1968) Terrestrial metamorphic clinoenstatite in kinks of bronzite crystals. Contributions to Mineralogy and Petrology, 19, 158–168.

Ulmer, P. and Trommsdorff, V. (1995) Serpentine stability to mantle depths and subduction-related magmatism. Science, 268, 858–861.

———(1999) Phase relations of hydrous mantle subducting to 300 km. In Y. Fei, C.M. Bertka, and B.O. Mysen, Eds, Mantle Petrology: field observations and high pressure experiments, p. 259–281. The Geochemical Society, Special Publication.

Woodland, A.B. (1998) The orthorhombic to high-P monoclinic phase transition in Mg-Fe pyroxenes: Can it produce a seismic discontinuity? Geophysical Research Letters, 25, 1241–1244.

Woodland, A.B. and Angel, R.J. (1997) Reversal of the orthoferrosilite—high-P ferrosilite transition, a phase diagram for $FeSiO_3$ and implications for the mineralogy of the Earth's upper mantle. European Journal of Mineralogy, 9, 245–254.

Wunder, B. and Schreyer, W. (1992) Metastability of the 10-Å phase in the system MgO-SiO_2-H_2O (MSH). What about hydrous MSH phases in subduction zones? Journal of Petrology, 33, 877–889.

———(1997) Antigorite: High-pressure stability in the system MgO-SiO_2-H_2O (MSH). Lithos, 41, 213–227.

Yagi, T. and Akimoto, S.-I. (1976) Direct determination of coesite-stishovite transition by in-situ X-ray measurements. Tectonophysics, 35, 259–270.

Yagi, T., Akaogi, M., Shimomura, O., Suzuki, T., and Akimoto, S.-I. (1987) In situ observation of the olivine-spinel phase transition in Fe_2SiO_4 using synchrotron. Journal of Geophysical Research, 92(B7), 6207–6213.

Yamamoto, K. and Akimoto, S.-I. (1977) The system MgO-SiO_2-H_2O at high pressures and temperatures-stability field for hydroxyl-chondrodite, hydroxyl-clinohumite and 10 Å-phase. American Journal of Science, 277, 288–312.

Zhang, J., Utsumi, W., and Liebermann, R.C. (1996) In situ X-ray observations of the coesite-stishovite transition: Reversed phase boundary and kinetics. Physics and Chemistry of Minerals, 23, 1–10.

MANUSCRIPT RECEIVED OCTOBER 10, 2000
MANUSCRIPT ACCEPTED JUNE 4, 2001
MANUSCRIPT HANDLED BY THOMAS DUFFY